Borghei, Maryam; Laocharoen, Nikorn; Kibena-Põldsepp, Elo; Johansson, Leena Sisko; Campbell, Joseph; Kauppinen, Esko; Tammeveski, Kaido; Rojas, Orlando J.

Porous N,P-doped carbon from coconut shells with high electrocatalytic activity for oxygen reduction

Published in:
Applied Catalysis B-Environmental

DOI:
10.1016/j.apcatb.2016.11.029

Published: 05/05/2017

Document Version
Peer-reviewed accepted author manuscript, also known as Final accepted manuscript or Post-print

Porous N,P-doped Carbon from Coconut Shells with High Electrocatalytic Activity for Oxygen Reduction: Alternative to Pt-C for Alkaline Fuel Cells

Maryam Borghei*[1], Nikorn Laocharoen[1], Elo Kibena-Põldsepp [2], Leena-Sisko Johansson[1], Joseph Campbell[1], Esko Kauppinen[3], Kaido Tammeveski[2], Orlando J. Rojas*[1,3]

[1]*Bio-Based Colloids and Materials, and Centre of Excellence on "Molecular Engineering of Biosynthetic Hybrid Materials Research" (HYBER), Department of Bioproducts & Biosystems, Aalto University, Finland*

[2]*Institute of Chemistry, University of Tartu, Estonia*

[3]*Nanomaterials Group, Department of Applied Physics, Aalto University, Finland*

Corresponding authors: maryam.borghei@aalto.fi, orlando.rojas@aalto.fi; Tel.: +358 5051 24227

KEYWORDS: Nitrogen-doped carbon; oxygen reduction reaction (ORR); coconut shells; electrocatalyst; fuel cells.

ABSTRACT

This study presents an environmentally-friendly method to synthesize N,P-doped porous carbon upon high conversion yield (46%) from bio-waste residues of coconut shells. The obtained materials displayed high electrocatalytic activity towards the oxygen reduction reaction, suitable as cathode catalyst for the alkaline fuel cells. The synthesis procedure included an efficient single-step activation with phosphoric acid to achieve high surface area of 1216 m^2 g^{-1} and pore volume 1.15 cm^3 g^{-1} with 72% mesopores. Urea was used as a low-cost and ecologically-sound source for nitrogen doping of the as-synthesized porous carbon. The biomass-derived electroactive carbon demonstrated a superior catalytic performance compared to a reference material, the state-of-the-art commercial Pt-C catalyst. The newly developed system displayed (a) comparable electrocatalytic activity, (b) better tolerance to methanol crossover effects and, (c) improved long-term durability towards oxygen reduction reaction in alkaline media.

1. INTRODUCTION

Fuel cells are promising and sustainable energy conversion alternatives owing to their zero or low greenhouse gas emission and high efficiency (~80%). However, the large scale application of fuel cells is limited by the need of incorporating expensive Pt-based catalysts in their cathodic and anodic electrode components [1,2]. Therefore, low-platinum or metal-free electrocatalysts are most desirable for fuel cells to enter the market [3]. Recently, nitrogen doping of carbon nanotubes (CNT) and graphene were reported to be beneficial to enhance the oxygen reduction reaction (ORR) in alkaline conditions [4]. Nitrogen doping effectively modulates the surface chemistry, electron-donor ability and electrochemical properties of the sp^2 carbon structure, as it has been confirmed by experiments and density functional theory (DFT) calculations [5], [6], [7], [8]. In addition, compared to single-atom doping, co-doping with other heteroatoms such as S, P and B improved the electrocatalytic activity for the ORR [9], [10].

Despite the outstanding properties of graphene and CNT, they are still expensive and their synthesis in large scale inherently involves the use of natural gas or hazardous chemicals, and metals as catalyst precursors [11]. Lignocellulosic biomass in the form of plant materials as well as wastes from household and animal husbandry is an abundant and renewable alternative for conversion to the novel value-added carbon products. Their use can additionally address issues related to waste disposal and accumulation. According to the United Nations, almost 140 billion metric tons of biomass is generated globally from agricultural waste [12]. Therefore, converting biomass can potentially reduce the use of fossil fuels as well as greenhouse gas release, while closing the carbon cycle loop and promoting economic incentives [13].

Nowadays, increasing attention is given towards porous carbons with electroactive properties produced from natural resources and lignocellulosic biomass. N-doped carbon materials have been synthesized for example from bacterial cellulose [14,15], cellulose nanocrystals [16], glucose and soy proteins [17], chitin [18],[19], chitosan [20], [21],[22] lignin [23], and plant biomass (*Eichhornia crassipes* [24] and *Typha orientalis* [25]). In addition, heteroatom-doped carbons have been explored, for example, via pyrolysis of cellulose phosphate

to yield P-doped carbon [26]; N,P-doped carbon from cellulose nanocrystals and ammonium phosphate [27]; N,S-doped carbon from human hair [28] or glucose and those derived from S-containing precursors such as S-(2-thienyl)-L-cysteine, 2-thienyl-carboxaldehyde, L-cysteine [29], [30]. The synthesis of multiple heteroatom-doped carbon has also been reported by direct pyrolysis of ginkgo leaves [31] and seaweeds [32].

Coconut shells represent an important bioresource in tropical areas, available in large quantities and display high carbon content and low ash residues (<1 wt.%) [33], [34]. Investigation of elemental composition showed that coconut shells contained higher content of carbon (~53-64 wt.%) and low H/C and O/C ratio that is due to the large lignin content (~30-49 wt.%) [35], [36], [37]. On the other hand, compared to the others agricultural biomass, the density of the raw coconut shells is among the highest (1.31) and the porosity is among the least (14.9 %) [37]. This means that the morphology of the plant cells of the coconut shell is more compact due to the stronger cross-linking of the cellulose, hemicellulose and lignin. Therefore, the coconut shells are reported to be more suitable raw material for production of activated carbon regarding the adsorption capacity, bulk density, pore structure and hardness. Recently, Yang et al. synthesized N-doped porous carbon for CO_2 adsorption with a micropore-dominant structure [38]. Despite the high adsorption capacity, the synthesis process involved multiple steps, such as separate carbonization and activation along with ammoxidation treatment (ammonia/air) for nitrogen doping. Zhao et al. suggested catalytic production of vinyl chloride on N-doped activated carbon by using melamine as N-containing precursor [39]. The present work is designed to obtain an electroactive N,P-doped mesoporous carbon via an economical and environmentally-sound process through a single-step activation with phosphoric acid, followed by nitrogen doping using urea. In valorization of biomass for development of novel catalytic materials, our aim is also to reduce the use of hazardous chemicals.

There are two main methods for the activation of lignocellulosic materials; either by physical or chemical processes [35]. Physical activation is carried out in two separate steps: a preliminary carbonization in an inert atmosphere at intermediate temperatures (400-500 °C), followed by activation using steam or carbon dioxide at higher temperatures (900-1000 °C) [40]. Chemical activation is done via impregnation of the raw material with given chemicals at specific ratios before carbonization. Potassium hydroxide (KOH), sodium hydroxide (NaOH), sodium carbonate (Na_2CO_3), magnesium chloride ($MgCl_2$), phosphoric acid (H_3PO_4) and zinc chloride ($ZnCl_2$) have been reported as typical dehydrating agents for chemical activation [41], [42], [43]. Phosphoric acid is an ideal reagent due to its low-cost, low environmental impact (milder than zinc chloride) and the possibility of producing high surface area carbon with desired pore size distribution, in a single-step and at low temperatures (400-500 ºC) [44]. It is also reported that the chemical activation of coconut shells with phosphoric acid can generate crack-free active carbon grains, leading to the better mechanical properties than the activated carbon via $ZnCl_2$ [35]. Urea is a non-toxic, cheap and an environmentally safe alternative among typical graphitic carbon nitride (g-C_3N_4) precursors such as thiourea, dicyandiamide and melamine [45]. Besides, urea presents a higher water solubility and can result in denser C-N sp^2 graphitic structures at

500 °C [46]. This study shows for the first time the development of N,P-doped porous carbons derived from coconut shells with high electrocatalytic activity towards the reduction of oxygen in alkaline media.

2. EXPERIMENTAL

2.1 Materials synthesis

The carbon samples were prepared after chemical activation of coconut shells with phosphoric acid, followed by doping with urea as nitrogen precursor and pyrolysis at 1000 ºC. In more detail, coconuts were purchased from a local market (S-Market, Finland) and their shells were grinded and sieved through 100 micron mesh. The powdered materials were chemically impregnated overnight with 50 wt.% H_3PO_4 (1:2 ratio), followed by drying at 70 ºC until a paste texture was obtained. The carbonization was carried out under nitrogen flow at 550 ºC for 1 h using a heating ramp rate of 10 ºC min^{-1}. The obtained carbon was washed with hot water and then immersed in 3 M HCl overnight and finally filtered and dried at 105 ºC. For nitrogen doping of the activated carbon (AC), a post-treatment was performed by dispersion in 1 M urea solution overnight. The resultant dispersion was filtered and dried, followed by pyrolysis at 1000 ºC for 2 h at 5 ºC min^{-1}. In order to enhance the interaction of urea with the activated carbon surface, the AC was treated with 2 M HNO_3/1 M H_2SO_4 (1:1 v/v) at 120 ºC for 2 h (functionalization treatment). Herein, the samples are coded as *AC* for activated carbon; *AC-P* for the *AC* after pyrolysis at 1000 ºC; *AC-U-P* for the impregnated *AC* with urea followed by pyrolysis and, finally, *AC-F-U-P* for the *AC* after functionalization and urea impregnation and pyrolysis. The schematic illustration of the synthesis procedure of the more complete sequence, *AC-F-U-P*, is provided in Figure 1.

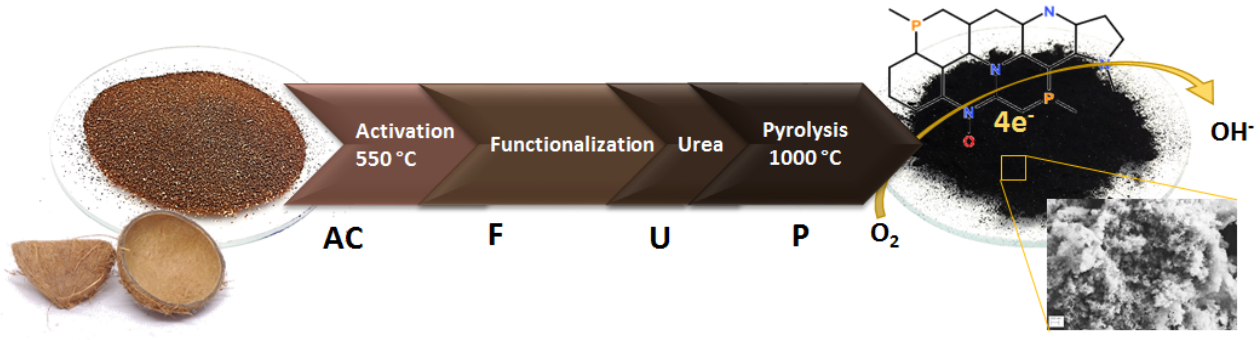

Figure 1. Schematic of the synthesis of N,P-doped porous carbon from coconut shells (*AC-F-U-P*). Shorter sequences are possible by skipping the functionalization (*F*) or urea treatment (*U*) steps.

2.2 Characterization

Scanning electron microscopy (SEM) studies were carried out with a field emission Zeiss Sigma VP at 2 kV. N_2 adsorption-desorption measurements were carried out at 77 K using a Micromeritics Tristar II equipped

with an automated surface area and pore size analyzer. Prior to the measurements, the samples were left in a degas system (Micromeritics II, Flow Prep 060) at 120 ºC for 2 h under N_2 flow. The Brunauer-Emmett-Teller (BET) method was used to determine the specific surface area, while Barrett-Joyner-Halenda (BJH) method and the DFT were applied to obtain the pore volume and pore size distributions. The total pore volume (V_T) was obtained from the adsorption value at relative pressure (p/p_0) of 0.99. X-ray photoelectron spectroscopy (XPS) was utilized for the surface chemical analysis of the prepared materials, using AXIS Ultra electron spectrometer (Kratos Analytical, UK) with monochromatic Al Kα irradiation (incident energy = 1486.6 eV) at 100 W and under neutralization. Both elemental wide spectra as well as high resolution regional spectra for carbon, oxygen and nitrogen were recorded. Thermal gravimetric analysis (TGA) was performed using a Perkin Elmer TGA7 system in a temperature range of 20-900 ºC at a heating rate of 10 °C min^{-1} under air condition. Raman spectroscopy was carried out using a Horiba LabRAM HR spectrometer equipped with CCD camera and 633 nm laser beam.

2.3 Electrochemical measurements

Catalyst inks were prepared by dispersing 15 mg of the respective carbon (*AC, AC-P, AC-U-P, AC-F-U-P*) in 476 µl of ethanol and 24 µl of FAA3 anion exchange ionomer (solution of 12 wt.% FAA3 in N-methyl-2-pyrrolydone, supplied by Fuma-Tech). Glassy carbon electrodes, GCE, (0.196 cm^2) were polished and a drop of 2 µl ink was deposited carefully to cover the whole surface. The modified GCE was dried under air flow and then in an oven at 60 ºC for 2 h. The half-cell electrochemical measurements were performed in a 3-electrode cell consisting the modified GCE as working electrode (WE), a Pt-rod as a counter electrode (CE) and a Ag/AgCl (3M KCl) as reference electrode (RE), controlled by an Autolab PGSTAT12 potentiostat (Metrohm-Autolab, The Netherlands) and General Purpose Electrochemical System (GPES) software. The ORR measurements were carried out by cyclic voltammetry (CV) in an O_2-saturated 0.1 M KOH electrolyte in a potential range from 0.2 to -1.2 V at scan rate of 10 mV s^{-1}. Rotating disk electrode (RDE) measurements were performed at different rotation rates from 100 to 2500 rpm at 10 mV s^{-1}. The durability of the samples was also evaluated by chronoamperometric measurements at -0.3 V for almost 50,000 s (~13 h). The ORR activity and stability of the catalysts were compared with the state-of-the-art commercial catalyst consisting of 20 wt.% Pt supported on carbon black (Pt-C), purchased from Alfa Aesar.

3. RESULTS AND DISCUSSION

3.1 Physicochemical characterization and heteroatom doping

The surface morphology of the activated carbon was studied using scanning electron microscope (SEM), as shown in Figure 2a. It can be seen that a highly porous, three-dimensional structure was created upon chemical activation with phosphoric acid. The N_2 adsorption isotherms and the pore distribution of *AC* and *AC-P* (Figure

2b and 2c) confirmed the high porosity that can be inferred from the SEM micrograph (Figure 2a). A type IV isotherm with a hysteresis loop at relative pressure > 0.4 indicated a dominant mesoporous structure. The low pressure region of the isotherm relates to the micropore filling, while the plateau at high relative pressures corresponds to the multilayer adsorption in the meso- and macropores. The specific surface area obtained for *AC* by the BET method was remarkable, 1216 m^2 g^{-1}, and the results included a large pore volume fraction (1.15 cm^3 g^{-1} with 72% of mesopores). The pore size distribution (Figure 2c) showed a sharp peak at ~2 nm, followed by wide distribution of mesopores with an average pore size of 4.8 nm (Figure 2d). The lack of isotherm plateau at high relative pressures together with the wide pore size distribution may indicate the slit-like pores in an open pore structure [29].

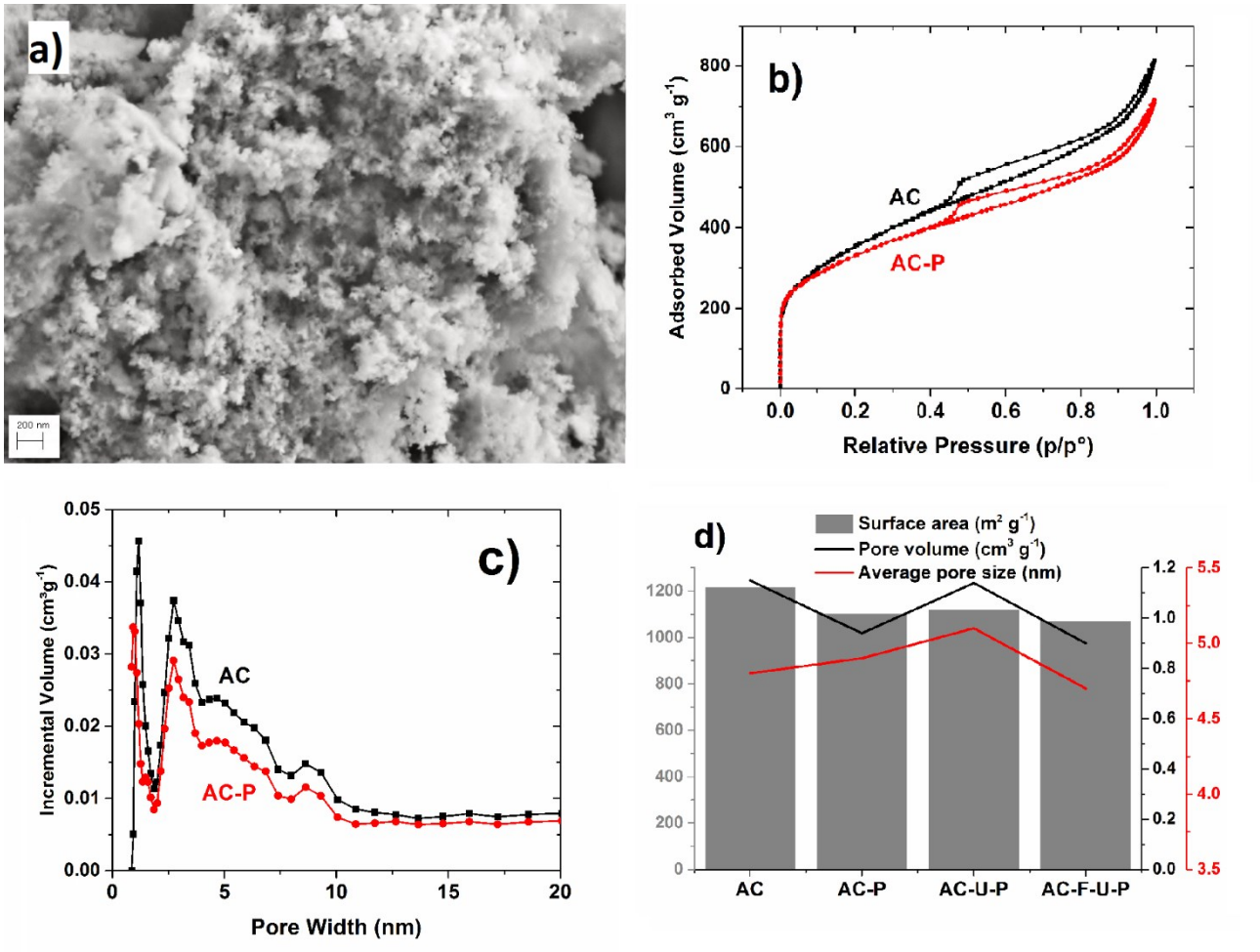

Figure 2. SEM micrograph of activated carbon (*AC*) after chemical activation of ground coconut shells (a). N_2 adsorption isotherms of *AC* and *AC-P* (b). Pore distribution of *AC* and *AC-P* from DFT method (c).

In general, several parameters such as the raw material, the activating chemical and its ratio, carbonization temperature, time and the ramp rate play a significant influence on the surface area and the pore structure of the activated carbon [47]. As mentioned above, coconut shell was chosen in this study due to the high carbon content, low ash and sufficient hardness which is essential for the final application as fuel cell electrocatalyst.

This is due to the morphology of the coconut shell plant cell which is more compact due to the stronger cross-linking of the cellulose, hemicellulose and lignin [37]. In activation via phosphoric acid, the phosphate and phosphate ester form linkages to the lignocellulose, thereby inhibit the shrinkage of the structure during the pyrolysis; as a result, the voids volume are protected [42]. Upon rinsing the sample after pyrolysis, the phosphate groups are washed away, forming large number of pores in the activated carbon structure. In addition, phosphoric acid retards the decomposition of lignocellulose by preventing tar formation and the evolution of volatile products during the pyrolysis, thus providing high carbonization yield (TGA analysis in Figure S1) [43]. Based on degradation temperature of impregnated coconut shells (Figure S1) and previous findings [48], the carbonization temperature was set at 550 °C in this study to obtain high *AC* yield (46%). Such high carbon yield is a crucial factor in the cost of the final electrocatalyst for fuel cells. We also observed that upon increasing the temperature ramp rate, higher mesopores content could be obtained (Figure S2), which is desirable for the application in this study. Phosphoric acid on one hand work as hydrolyzing agent to cleave the lignocellulosic bonds, and on the other hand as cross-linker via formation of phosphate ester linkages. Upon heat treatment of the lignocellulos-phosphoric acid mixture, initially crosslinking reactions dominate over bond cleavage until ~250 °C. As the temperature increased, cyclization and condensation overcomes due to the scission of P-O-C bonds. In a faster heating ramp, the rate of phosphate bond cleavage occurs faster than the condensation and reordering of the clusters, leaving larger pores [49]. Therefore, a 10 °C min^{-1} heating rate was chosen to obtain wider mesopores contribution, with additional benefit of decreasing the activation cost.

In the case of *AC-P*, heat-treatment of *AC* at 1000 ºC (2 h) did not influence the pore structure. The BET surface area and pore volume of *AC-P* only decreased slightly, owing to carbon gasification. Interestingly, the N_2 adsorption isotherms and pore size distribution of *AC-U-P* and *AC-F-U-P* (Figure S3) did not significantly change after further processing via acid functionalization (120 ºC, 2 h) and urea impregnation. However, longer functionalization for 4 h significantly damaged the pore structure (Figure S4). Treatment with urea prevented gasification, possibly due to crosslinking and formation of graphitic carbon nitride sheets [50]. Notably, the pore structure and surface area of *AC-F-U-P* was still similar to that of the other samples (Figure 2d), even after functionalization treatment. This indicated a high mechanical strength of the activated carbon produced from the coconut shells [51].

The XPS survey spectrum of the carbon samples (Figure 3a) shows a strong carbon C1s peak at 284.3 eV as well as signals for oxygen (O1s at around 532 eV) and phosphorus (P2p at 133 eV and P2s at 190.3 eV) [26],[27]. According to the asymmetric shape of the sharp peak at 284.3 eV in the C1s high resolution spectrum (Figure S5), carbon was exclusively in graphitic form. In the high resolution spectrum of oxygen (Figure S5) both carbon- and phosphorus-bonded atoms (or surface hydroxyls due to exposure to air) were seen as the O1s signal was split into two components at 532.8 and 530.5 eV. The quantitative analysis (Figure 3b) showed that phosphorus content is about 2.3 at.%, a relatively large content that resulted from effective chemical activation

with phosphoric acid. Interestingly, phosphorus content did not change after functionalization and urea treatment, suggesting strong bonds within the carbon framework (Figure 3b).

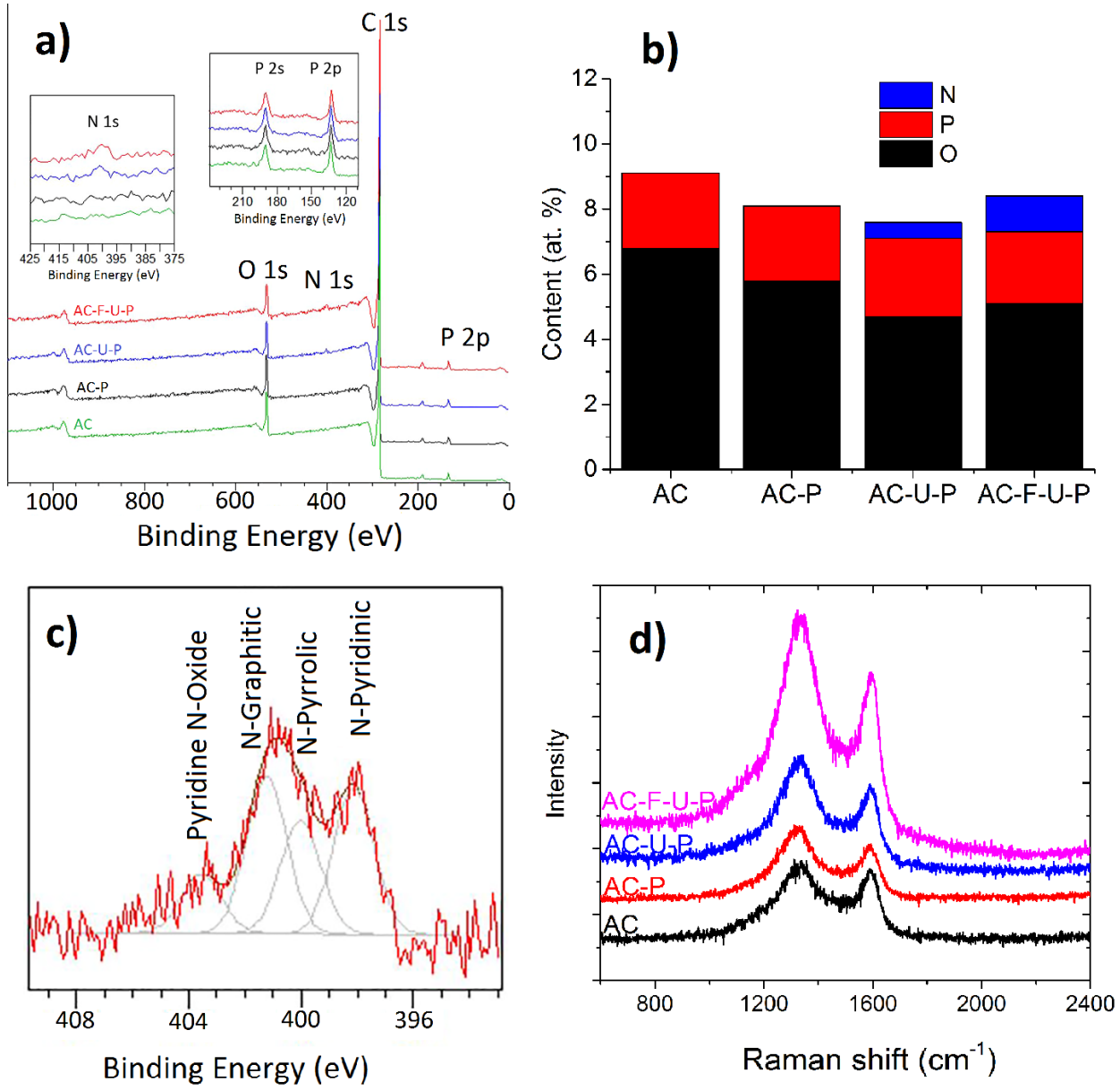

Figure 3. XPS survey spectra of carbon samples (inset: high-resolution N*1s* and P*2p* spectra) (a). Atomic % of elements present on the surface according to XPS (b). Deconvolution of high-resolution N*1s* spectra with assigned N-functionalities (c) and Raman spectra of *AC, AC-P, AC-U-P, AC-F-U-P* samples (d).

A small N1s peak at ca. 400 eV (Figure 3a) was evident in *AC-U-P* and *AC-F-U-P* samples, suggesting N-doping of the activated carbons after impregnation with urea. The nitrogen content almost doubled from 0.5 at.% *(AC-U-P*) to 1.1 at.% (*AC-F-U-P*), upon functionalization and enhanced interaction of urea with oxygen functional groups on the surface (Figure 3b). A slight but measurable decrease in the O/C atomic ratio, from 0.06 (*AC-P*) to 0.05 (*AC-U-P*), was observed upon urea addition. The close relationship between the nitrogen doping and disappearance of oxygen-containing moieties suggests the occurrence of reactions of oxygen

functional groups with the amine groups of urea [50]. This was also observed in FTIR spectra (Figure S6). The deconvolution of N1s peak of *AC-F-U-P* (Figure 3c) showed the presence of four types of N-functionalities including N-pyridinic (398.4 eV, 31.1 at.%), N-pyrrolic (399.8 eV, 24.8 at.%), N-graphitic (401.5 eV, 33.6 at.%) and pyridine N-oxide (402.9 eV, 10.5 at.%). The high concentration of N-graphitic may be the result of the graphitic carbon nitride originated from urea and also the partial transformation of N-pyridinic into N-graphitic as the pyrolysis temperature increases to 1000 ºC, due to the condensation of graphitic rings [52]. The N-pyridinic and N-graphitic have been recognized to impart high electrocatalytic activity for the ORR [53].

Raman spectra indicated the influence of N-doping treatments on the carbon structure (Figure 3d). The D-band, the characteristic breathing mode of aromatic rings, occurred at 1340 cm^{-1}. The G-band, around 1590 cm^{-1}, assigned to the tangential vibration mode of carbon atoms. A high I_D/I_G ratio is typically indicative of more disordered carbon structures [54], [55]. In the present case, the I_D/I_G values for *AC* and *AC-P* were similar ~1.1; however, it increased to 1.25 for *AC-U-P*. It is well-known that the addition of heteroatoms in the graphitic carbon lattice structure results in more defects and a larger D-band intensity [56]. As expected further functionalization in *AC-F-U-P* created more defects, and resulted in an increased I_D/I_G value (~1.4).

3.2 Electrochemical activity

The oxygen reduction reaction (ORR) in aqueous solutions mainly occur through different pathways: a direct 4-electron reduction from O_2 to H_2O (OH^- in alkaline), and the 2-electron reduction to H_2O_2 (HO^-_2 in alkaline) [57]:

4-electron process: $O_2 + 2H_2O + 4e^- \rightarrow 4OH^-$

2-electron process: $O_2 + H_2O + 2e^- \rightarrow HO_2^- + OH^-$

$$HO_2^- + H_2O + 2e^- \rightarrow 3OH^-$$

The electrocatalytic activity of the catalysts toward the ORR was first evaluated by cyclic voltammetry (CV) (Figure 4a). Cyclic voltammogram of *AC-P* in O_2-sturated 0.1 M KOH clearly showed characteristic two step 2-electron reduction process, with peak potentials occurring at -0.23 and -0.6 V. In the case of *AC-U-P* electrode, the treatment with urea slightly improved the ORR activity (Figure 4a). However, functionalization of the active carbon before pyrolysis enhanced the catalytic activity of *AC-F-U-P* by shifting the ORR peak potential to a more positive value (-0.15 V). Linear scan voltammograms (LSV) were recorded from the RDE measurements for each catalyst (Figure 4b). The baseline currents were recorded in the absence of oxygen and subtracted from the polarization curves recorded in the O_2-saturated electrolyte, allowing determination of the onset potential for ORR. A shift of the onset potential towards more positive potentials, from -0.17 V (AC-P)

to -0.15 V (AC-U-P) was observed. This transition further improved to -0.02 V for *AC-F-U-P*, much closer to the commercial Pt-C onset potential (0.05 V).

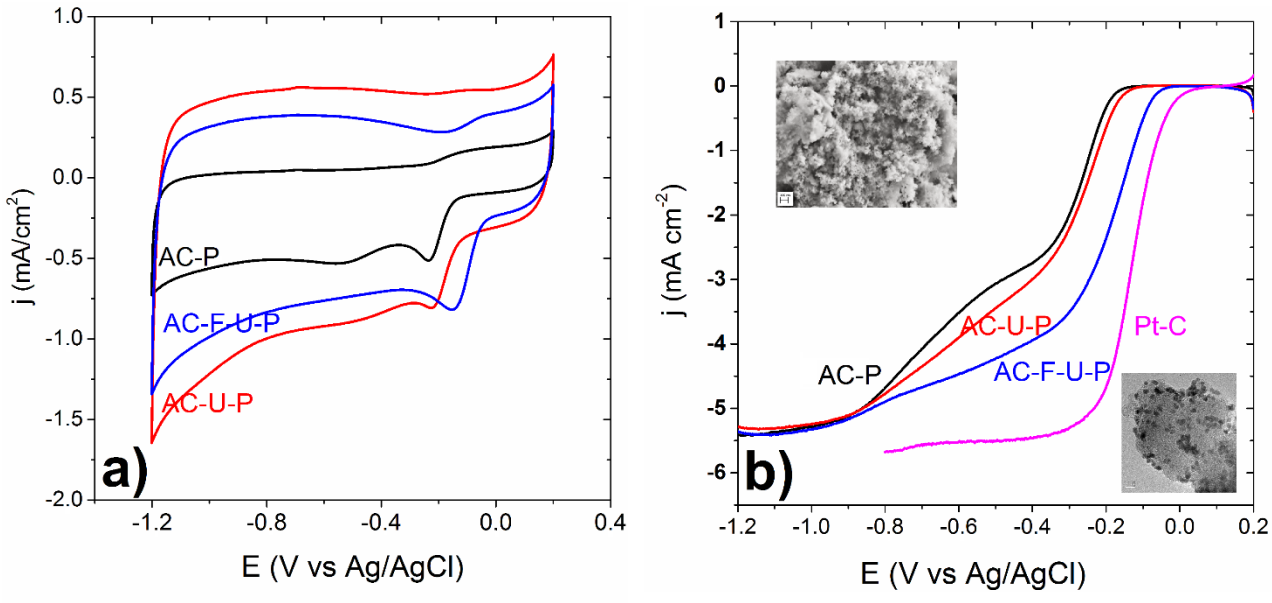

Figure 4. CV recorded at 10 mV s^{-1} (a) and LSV at 1600 rpm in O_2-sturated 0.1 M KOH (b) of carbon samples derived from coconut shells, as indicated (the profile for commercial Pt-C is included for comparison).

In order to quantify the kinetics of the ORR, the Koutecky-Levich (K-L) plots were derived from the LSV profiles at different rotation rates. The LSV profiles of *AC-F-U-P* at different rotation rates and the corresponding K-L plots at different potentials are presented in Figure 5. The K-L plots were linear and near parallel, indicating a first-order reaction kinetics toward the ORR, and a similar electron transfer number (*n*) at the different potentials. The value of *n* can be calculated from the K-L equation [58]:

$$\frac{1}{j} = \frac{1}{j_k} + \frac{1}{j_d} = \frac{1}{j_k} + \frac{1}{0.62nFD_{O_2}^{2/3}\nu^{-1/6}C_{O_2}^{b}\omega^{1/2}}$$

where j is the overall current density, and j_k and j_d are the kinetic and diffusion-limited current densities, respectively. ω is the electrode rotation rate (rad s^{-1}), F is the Faraday constant (96486.4 C mol^{-1}); C_{O2} is the concentration of O_2 in 0.1 M KOH (1.26×10^{-6} mol cm^{-3}); D_{O2} is the diffusion coefficient of O_2 in 0.1 M KOH (1.9×10^{-5} cm^2 s^{-1}); ν is the kinematic viscosity of the electrolyte (0.01 cm^2 s^{-1}) [57].

The K-L plots for *AC* and *AC-P* (measured at -0.4 V) are presented for comparison in Figure 5c, together with that of *AC-F-U-P*. The *n* value for all the samples was calculated from the slope of the K-L curves at the different potentials, and compared with that for the commercial Pt-C electrode (Figure 5d). The average number of transferred electrons in the potential range between -0.3 and -0.5 V showed a significant improvement upon urea treatment: from n = 2.7 (*AC-P*) to 3.2 (*AC-U-P*), a remarkable change only with 0.5

at.% of nitrogen doping level. The value of *n* was further enhanced to ~3.7 for *AC-F-U-P*, after functionalization was performed on the activated carbon.

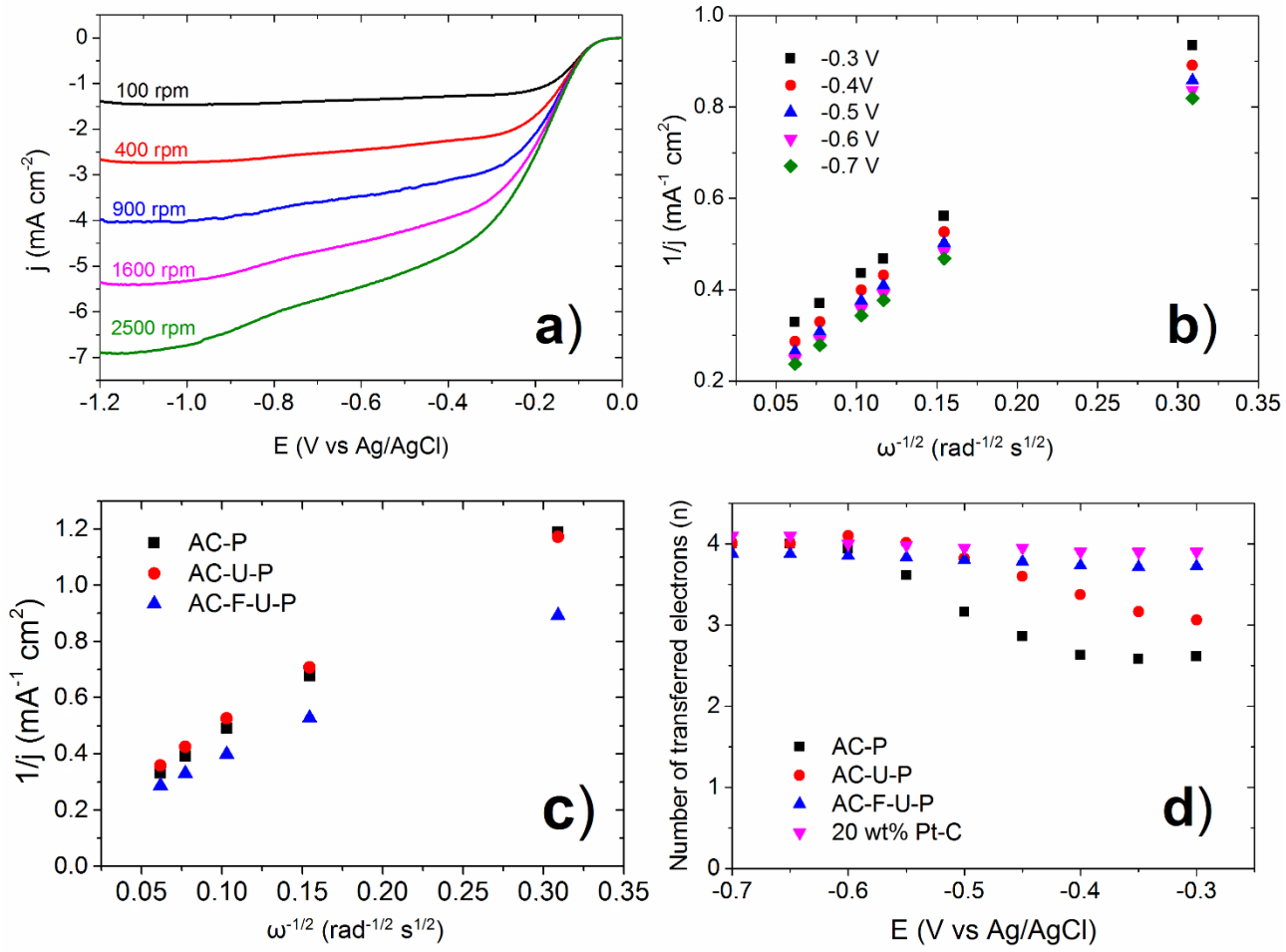

Figure 5. LSV curves for the AC-F-U-P sample at different rotation rates in O_2-saturated 0.1 M KOH (a), K-L plots derived from (a) at different potentials (b), K-L plots at -0.4 V for *AC*, *AC-P* and *AC-F-U-P* derived from the respective LSV curves (c), and the electron transfer number calculated from the K-L equation at different potentials (d).

It can be also concluded that the functionalization treatment made a significant effect on the ORR electrocatalytic activity by providing more oxygen-containing functional groups on the surface of the activated carbon, which interact with urea and, consequently, increases the N-doping level. This effect has been also reported earlier for few-walled carbon nanotubes (FWCNTs) when polyaniline (PANI) was used as nitrogen precursor, leading to a significantly enhanced ORR activity upon functionalization of pristine FWCNTs before doping with PANI [53].

The better ORR electrocatalytic activity observed at *AC-F-U-P* for ORR can be explained by the higher N content (1.1 at.%) in this sample. The exact role of nitrogen and its influence on the reduction of oxygen is still a controversial subject. In some cases, a direct correlation between N-doping level and an improved ORR activity has been observed [59], [60]; while in contrast, others have found no relation between the higher total nitrogen content and the ORR activity [61], [59]. For example, a high ORR electrocatalytic activity (n = 3.7)

was observed with very low nitrogen doping levels (0.5 at.%) in N-doped FWCNTs [53], [62]. While in another study, N-CNTs containing nitrogen as high as 20 at.% provided much lower ORR catalytic activity (*n*: 2.6) [63]. Comparison of the ORR activity of *AC-F-U-P* obtained from coconut shells to the N-doped carbon from different types of biomass is provided in Table 1.

Table 1. Comparison of the biomass-derived nitrogen-doped carbon materials for the ORR.

Carbon precursor	**Nitrogen precursor**	**Activating agent**	**Pyrolysis Temp. (°C)**	**surface area (m^2 g^{-1})**	**Pore volume (cm^3 g^{-1})**	**Total N, P/S (at. %)**	**Electron transferred (*n*)**	**Ref.**
Cellulose nanocrystals	Urea	--	1000	1362.36	3.36	3.51	--	[16]
Glucose/ Cellulose microcrystalline	Soy protein	--	1000	449 697	0.25 0.38	1.9 0.5	3.5 3.3	[17]
Chitin	--	$ZnCl_2$	750	300.7	0.31	4.99	3.93	[19]
Chitosan	Urea	--	1000	1510	1.32	4.36	3.67	[22]
Eichhornia crassipes	--	$ZnCl_2$	800	950.6	1.49	4.76	3.51-3.82	[24]
Typha orintalis	NH_3	--	800	898	0.52	9.1	3.7-4	[25]
Cellulose microcrystalline	$(NH_4)_3PO_4$	--	900	--	--	N:2.17 P:2.22	3.5	[27]
Human hair	--	NaOH	900	1813.65	--	N:3.8 S:1.7	3.8-3.9	[28]
Ginkgo leaves	NH_3	--	1000	1436.02	--	1.59	3.7	[31]
Seaweed	--	--	1000	1217-78	1.45	2.3	3.7	[32]
Coconut shells	Urea	H_3PO_4	1000	1071	0.9	N:1.1 P:2.3	3.7	This work

The excellent electrocatalytic performance of the activated carbon obtained from coconut shells can also be ascribed to the high surface area and the large contribution of mesopores. Both factors enhance the mass transport of the liquid electrolyte. The governing influence of surface area on the catalytic activity (rather than the nitrogen content) was previously reported by Jaouen et al. [64]. The three-dimensional open pore structure provides enhanced accessibility of the oxygen molecules to the active sites [65], despite the low N content, together with the synergistic effect of P-heteroatom in the structure as reported earlier. Taken together, the observations point to an ORR mechanism of the activated carbons involving an electron transfer number close to 4 (pseudo-4e^- mechanism), even with low nitrogen doping level. According to our previous findings, in the porous N-doped carbons with low nitrogen content, the adsorption of O_2 molecules likely occurs on N-

graphitic sites [5], followed by a fast decomposition or an electroreduction of hydroperoxide on N-pyridinic, overall leading to a fast conversion of oxygen molecules [65].

3.3 Electrode stability and methanol tolerance

The long-term stability of the carbon samples was evaluated by chronoamperometry at -0.3 V (900 rpm for 50,000 s) (Figure 6a). *AC-P* retained almost 90% of its initial activity after 13 h in continuous operation. Treatment with urea (*AC-U-P*) only slightly degraded the durability to 85%. However, functionalization that effectively increased the electroactivity undermined the electrode stability, reaching a plateau of about 75% after 13 h for *AC-F-U-P*.

It is possible that the severe acid treatment performed on the activated carbon created more defects in the structure, as observed by Raman spectroscopy, leading to catalyst deactivation with time. However, we note that the decrease in current response can also be a consequence of detachment of the catalyst particles from the surface of the GCE, a highly probable factor given the high rotation speed during the 13 h-long test, as has been reported elsewhere [46]. Nevertheless, the durability of *AC-F-U-P* as measured by the performance after 13 h was close to that of the commercial Pt-C electrode. Furthermore, any possible degradation of *AC-F-U-P* seemed to slow down with time (plateau profile) while the degradation of Pt-C displayed a sharp slope to lower values. It is known that Pt-C deactivation occurs due to the susceptible oxidation or loss of Pt nanoparticles as well as the corrosion of the carbon black support. Overall, the stability of the developed nitrogen-doped electrocatalyst obtained from coconut shells is similar to the range of values reported for N-doped carbons from biomass, about 80-85% [25], [28], [31], [46], but excels in the fact that the ORR activity is close to that measured for Pt-C used for benchmarking.

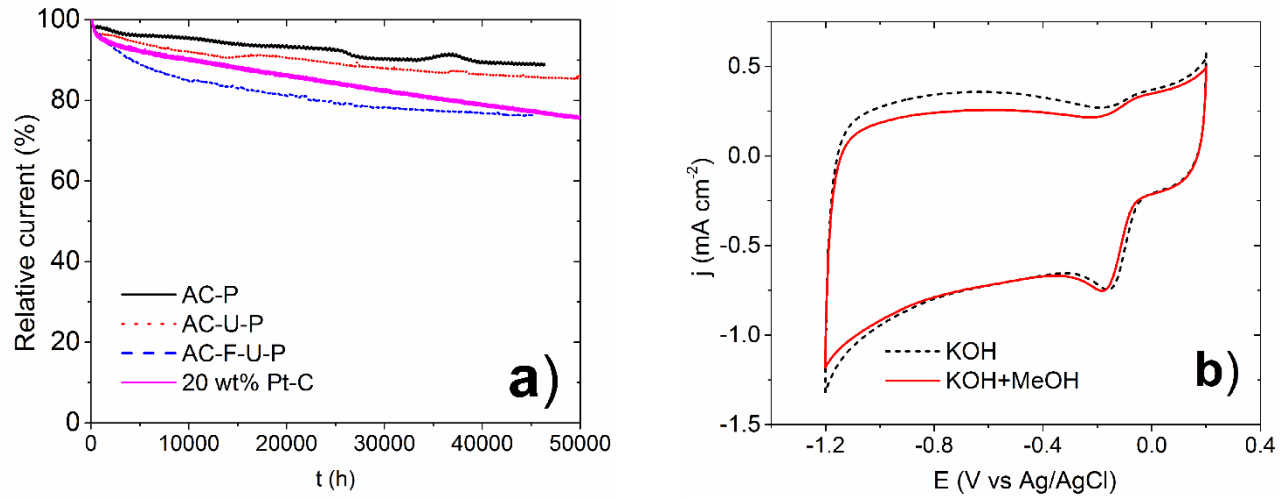

Figure 6. Stability measurement by chronoamperometry at -0.3 V at 900 rpm for 13 h (a), methanol oxidation assessment for *AC-F-U-P* electrode with and without the presence of methanol (3 M) in O_2-saturated 0.1 M KOH.

The tolerance of *AC-F-U-P* against methanol crossover was assessed in O_2-saturated 0.1 M KOH containing 3 M methanol (Figure 6b). In the presence of methanol, the catalyst responded with the same peak current/position compared to the pure KOH electrolyte. This suggests excellent selectivity of *AC-F-U-P* toward the ORR, in contrast to Pt-C catalyst where a large current response was always observed (Figure S7). Thus, as important advantage of the developed material is that it does not suffer from the major drawback observed in other systems with regards to the effect of methanol oxidation; i.e. the crossover issue in the case of Pt-C, that is methanol passing through the membrane, from the anode to the cathode compartment of the fuel cell, and methanol oxidation that competes for active sites as well as Pt-C catalyst CO poisoning [66].

4. Conclusions

Herein, a facile and cost-effective route for the valorization of waste biomass toward electroactive materials is demonstrated. Coconut shells were chosen due to the high lignin and low ash content in order to obtain higher product yield. Activated carbons were obtained in high yields (46%) by an optimized activation of coconut shells via phosphoric acid at mild temperatures (550 ºC). The resulting carbon structures displayed high porosity (1260 $m^2 g^{-1}$ specific surface area, 1.15 $cm^3 g^{-1}$ pore volume) and large mesopore volume (72%). Urea was used as a low-cost and ecologically-sound nitrogen source for improved electrocatalytic activity in ORR; it thus enabled N-doping of the activated carbon structure after pyrolysis. Despite a relatively low nitrogen content, a high ORR activity was measured upon functionalization of the coconut-derived carbon, comparable to that of a reference commercial Pt-C catalyst. Moreover, the porous carbon catalysts showed excellent long-term stability and tolerance toward methanol oxidation. Such exceptional catalytic performance can be ascribed to the unique hierarchical porous structure of the obtained materials, which also benefit from (a) the contribution of a large fraction of mesopores that provides enhanced electrolyte mass transport and easy access of oxygen molecules to the active sites; (b) the synergic effect of N and P doping, and (c) large proportion of active nitrogen species (N-graphitic and N-pyridinic). The prepared material is not only promising alternative to Pt-containing electrocatalysts for alkaline fuel cells, but also would be attractive material for other applications such as supercapacitors, catalytic conversion, electrochemical sensors and gas sorbents.

ACKNOWLEDGMENT

The authors would like to thank the Academy of Finland center of excellence in "Molecular Engineering of Bio-synthetic materials" (HYBER) for funding the project. This work made use of the Aalto University Nanomicroscopy Center. This research was also supported by institutional funding (IUT20-16) of the Estonian Ministry of Education and Research and by the EU through the European Regional Development Fund (TK141 “Advanced materials and high-technology devices for energy recuperation systems”).

REFERENCES

[1] W.Y. Wong, W.R.W. Daud, A.B. Mohamad, A.A.H. Kadhum, E.H. Majlan, K.S. Loh, Nitrogen-containing carbon nanotubes as cathodic catalysts for proton exchange membrane fuel cells, Diam. Relat. Mater. 22 (2012) 12–22.

[2] X. Zhao, M. Yin, L. Ma, L. Liang, C. Liu, J. Liao, T. Lu, W. Xing, Recent advances in catalysts for direct methanol fuel cells, Energy Environ. Sci. 4 (2011) 2736.

[3] F. Jaouen, E. Proietti, M. Lefèvre, R. Chenitz, J.-P. Dodelet, G. Wu, H.T. Chung, C.M. Johnston, P. Zelenay, Recent advances in non-precious metal catalysis for oxygen-reduction reaction in polymer electrolyte fuel cells, Energy Environ. Sci. 4 (2011) 114.

[4] D. Yu, E. Nagelli, F. Du, L. Dai, Metal-free carbon nanomaterials become more active than metal catalysts and last longer, J. Phys. Chem. Lett. 1 (2010) 2165–2173.

[5] D. Srivastava, T. Susi, M. Borghei, L. Kari, Dissociation of oxygen on pristine and nitrogen-doped carbon nanotubes: a spin-polarized density functional study, RSC Adv. 4 (2014) 15225–15235.

[6] P. Ayala, R. Arenal, M. Rümmeli, A. Rubio, T. Pichler, The doping of carbon nanotubes with nitrogen and their potential applications, Carbon N. Y. 48 (2010) 575–586.

[7] M. Terrones, A.G.S. Filho, A.M. Rao, Doped Carbon Nanotubes : Synthesis , Characterization and Applications, Springer, B. Chapter. 566 (2008) 531–566.

[8] S. Ni, Z.Y. Li, J.L. Yang, Oxygen molecule dissociation on carbon nanostructures with different types of nitrogen doping, Nanoscale. 4 (2012) 1184–1189.

[9] V. V. Strelko, V.S. Kuts', The effect of nitrogen in the carbon matrix on the donor-acceptor and catalytic activity of activated carbons in electron transfer reactions, Theor. Exp. Chem. 35 (1999) 315–318.

[10] D. Yu, Y. Xue, L. Dai, Vertically Aligned Carbon Nanotube Arrays Co-doped with Phosphorus and Nitrogen as E ffi cient Metal-Free Electrocatalysts for Oxygen Reduction, J. Phys. Chem. Lett. 3 (2012) 2863–2870.

[11] K.A. Shah, B.A. Tali, Synthesis of carbon nanotubes by catalytic chemical vapour deposition: A review on carbon sources, catalysts and substrates, Mater. Sci. Semicond. Process. 41 (2016) 67–82.

[12] J. United Nations Environmental Programme Division of Technology, Industry and Economics International Environmental Technology Centre Osaka/Shiga, C onverting W aste A gricultural B iomass into a R esource, United Nations Environ. Program. (2009) 1–437.

[13] S. De, A.M. Balu, J.C. Van Der Waal, R. Luque, Biomass-derived porous carbon materials: Synthesis

and catalytic applications, ChemCatChem. 7 (2015) 1608–1629.

[14] C. Long, D. Qi, T. Wei, J. Yan, L. Jiang, Z. Fan, Nitrogen-doped carbon networks for high energy density supercapacitors derived from polyaniline coated bacterial cellulose, Adv. Funct. Mater. 24 (2014) 3953–3961.

[15] L.F. Chen, Z.H. Huang, H.W. Liang, H.L. Gao, S.H. Yu, Three-dimensional heteroatom-doped carbon nanofiber networks derived from bacterial cellulose for supercapacitors, Adv. Funct. Mater. 24 (2014) 5104–5111.

[16] Q. Liu, C. Chen, F. Pan, J. Zhang, Highly efficient oxygen reduction on porous nitrogen-doped nanocarbons directly synthesized from cellulose nanocrystals and urea, Electrochim. Acta. 170 (2015) 234–241.

[17] S.-M. Alatalo, K. Qiu, K. Preuss, A. Marinovic, M. Sevilla, M. Sillanpää, X. Guo, M.-M. Titirici, Soy protein directed hydrothermal synthesis of porous carbon aerogels for electrocatalytic oxygen reduction, Carbon N. Y. 96 (2016) 622–630.

[18] T.-D. Nguyen, K.E. Shopsowitz, M.J. MacLachlan, Mesoporous nitrogen-doped carbon from nanocrystalline chitin assemblies, J. Mater. Chem. A. 2 (2014) 5915–5921.

[19] H. Yuan, L. Deng, X. Cai, S. Zhou, Y. Chen, Y. Yuan, RSC Advances Nitrogen-doped carbon sheets derived from chitin as non-metal bifunctional electrocatalysts for oxygen reduction and evolution †, RSC Adv. 5 (2015) 56121–56129.

[20] A. Primo, P. Atienzar, E. Sanchez, J.M. Delgado, H. García, From biomass wastes to large-area, high-quality, N-doped graphene: catalyst-free carbonization of chitosan coatings on arbitrary substrates, Chem. Commun. 48 (2012) 9254.

[21] M.K. Rybarczyk, M. Lieder, M. Jablonska, N-doped mesoporous carbon nanosheets obtained by pyrolysis of a chitosan–melamine mixture for the oxygen reduction reaction in alkaline media, RSC Adv. 5 (2015) 44969–44977.

[22] Q. Liu, Y. Duan, Q. Zhao, F. Pan, B. Zhang, J. Zhang, Direct Synthesis of Nitrogen-Doped Carbon Nanosheets with High Surface Area and Excellent Oxygen Reduction Performance, Langmuir. 30 (2014) 8238–8245.

[23] Y. Yang, Y. Deng, Z. Tong, C. Wang, Renewable lignin-based xerogels with self-cleaning properties and superhydrophobicity, ACS Sustain. Chem. Eng. 2 (2014) 1729–1733.

[24] X. Liu, Y. Zhou, W. Zhou, L. Li, S. Huang, S. Chen, Biomass-derived nitrogen self-doped porous carbon as effective metal-free catalysts for oxygen reduction reaction, Nanoscale. 7 (2015) 6136–6142.

[25] P. Chen, L.-K. Wang, G. Wang, M.-R. Gao, J. Ge, W.-J. Yuan, Y.-H. Shen, A.-J. Xie, S.-H. Yu, Nitrogen-doped nanoporous carbon nanosheets derived from plant biomass: an efficient catalyst for oxygen reduction reaction, Energy Environ. Sci. 7 (2014) 4095–4103.

[26] Q. Liu, S. Chen, Y. Zhou, S. Zheng, H. Hou, F. Zhao, Phosphorus-doped carbon derived from cellulose phosphate as efficient catalyst for air-cathode in microbial fuel cells, J. Power Sources. 261 (2014) 245–248.

[27] Q. Liu, Y. Zhou, S. Chen, Z. Wang, H. Hou, F. Zhao, Cellulose-derived nitrogen and phosphorus dual-doped carbon as high performance oxygen reduction catalyst in microbial fuel cell, J. Power Sources. 273 (2015) 1189–1193.

[28] K.N. Chaudhari, M.Y. Song, J.S. Yu, Transforming hair into heteroatom-doped carbon with high surface area, Small. 10 (2014) 2625–2636.

[29] S.-A. Wohlgemuth, R.J. White, M.-G. Willinger, M.-M. Titirici, M. Antonietti, A one-pot hydrothermal synthesis of sulfur and nitrogen doped carbon aerogels with enhanced electrocatalytic activity in the oxygen reduction reaction, Green Chem. 14 (2012) 1515.

[30] L. Roldan, Y. Marco, E. Garcia-Bordeje, Bio-sourced mesoporous carbon doped with heteroatoms (N,S) synthesised using one-step hydrothermal process for water remediation, Microporous Mesoporous Mater. 222 (2016) 55–62.

[31] F. Pan, Z. Cao, Q. Zhao, H. Liang, J. Zhang, Nitrogen-doped porous carbon nanosheets made from biomass as highly active electrocatalyst for oxygen reduction reaction, J. Power Sources. 272 (2014) 8–15.

[32] M.Y. Song, H.Y. Park, D.S. Yang, D. Bhattacharjya, J.S. Yu, Seaweed-derived heteroatom-doped highly porous carbon as an electrocatalyst for the oxygen reduction reaction, ChemSusChem. 7 (2014) 1755–1763.

[33] K. Yang, J. Peng, C. Srinivasakannan, L. Zhang, H. Xia, X. Duan, Preparation of high surface area activated carbon from coconut shells using microwave heating, Bioresour. Technol. 101 (2010) 6163–6169.

[34] W. Li, K. Yang, J. Peng, L. Zhang, S. Guo, H. Xia, Effects of carbonization temperatures on characteristics of porosity in coconut shell chars and activated carbons derived from carbonized coconut shell chars, Ind. Crops Prod. 28 (2008) 190–198.

[35] M.J. Prauchner, F. Rodríguez-Reinoso, Chemical versus physical activation of coconut shell: A comparative study, Microporous Mesoporous Mater. 152 (2012) 163–171.

[36] T. Rout, D. Pradhan, R.K. Singh, N. Kumari, Exhaustive study of products obtained from coconut

shell pyrolysis, J. Environ. Chem. Eng. 4 (2016) 3696–3705.

[37] W. Heschel, E. Klose, On the suitability of agricultural by-products for the manufacture of granular activated carbon, FuelVol. 74 (1995) 1786–1791.

[38] M. Yang, L. Guo, G. Hu, X. Hu, L. Xu, J. Chen, W. Dai, M. Fan, Highly cost-effective nitrogen-doped porous coconut shell-based CO2 sorbent synthesized by combining ammoxidation with KOH activation, Environ. Sci. Technol. 49 (2015) 7063–7070.

[39] W. Zhao, M. Sun, H. Zhang, Y. Dong, X. Li, W. Li, J. Zhang, Catalytic dehydrochlorination of 1,2-dichloroethane to produce vinyl chloride over N-doped coconut activated carbon, RSC Adv. 5 (2015) 104071–104078.

[40] J. Mi, X.-R. Wang, R.-J. Fan, W.-H. Qu, W.-C. Li, Coconut-Shell-Based Porous Carbons with a Tunable Micro/ Mesopore Ratio for High-Performance Supercapacitors, Energy and Fuels. 26 (2012) 5321–5329.

[41] A. Jain, S.K. Tripathi, Fabrication and characterization of energy storing supercapacitor devices using coconut shell based activated charcoal electrode, Mater. Sci. Eng. B. 183 (2014) 54–60.

[42] R.G. Pereira, C.M. Veloso, N.M. da Silva, L.F. de Sousa, R.C.F. Bonomo, A.O. de Souza, M.O. da G. Souza, R. da C.I. Fontan, Preparation of activated carbons from cocoa shells and siriguela seeds using H3PO4 and ZnCL2 as activating agents for BSA and α-lactalbumin adsorption, Fuel Process. Technol. 126 (2014) 476–486.

[43] W.C. Lim, C. Srinivasakannan, N. Balasubramanian, Activation of palm shells by phosphoric acid impregnation for high yielding activated carbon, J. Anal. Appl. Pyrolysis. 88 (2010) 181–186.

[44] X. Wang, D. Li, W. Li, J. Peng, H. Xia, L. Zhang, S. Guo, G. Chen, Optimization of mesoporous activated carbon from coconut shells by chemical activation with phosphoric acid, BioResources. 8 (2013) 6184–6195.

[45] G. Dong, Y. Zhang, Q. Pan, J. Qiu, A fantastic graphitic carbon nitride (g-C3N4) material: Electronic structure, photocatalytic and photoelectronic properties, J. Photochem. Photobiol. C Photochem. Rev. 20 (2014) 33–50.

[46] Q. Liu, Y. Duan, Q. Zhao, F. Pan, B. Zhang, J. Zhang, Direct Synthesis of Nitrogen-Doped Carbon Nanosheets with High Surface Area and Excellent Oxygen Reduction Performance. Langmuir 30 (2014) 8238-8245.

[47] T. Khadiran, M.Z. Hussein, Z. Zainal, R. Rusli, Textural and Chemical Properties of Activated Carbon Prepared from Tropical Peat Soil by Chemical Activation Method, Bioresources. 10 (2015) 986–1007.

[48] S. Ouyang, S. Xu, N. Song, S. Jiao, Coconut shell-based carbon adsorbents for ventilation air methane enrichment, Fuel. 113 (2013) 420–425.

[49] M. Jagtoyen, F. Derbyshire, Activated carbons from yellow poplar and white oak by H3PO4 activation, Carbon N. Y. 36 (1998) 1085–1097.

[50] Z.-H. Sheng, L. Shao, J.-J. Chen, W.-J. Bao, F.-B. Wang, X.-H. Xia, Catalyst-Free Synthesis of Nitrogen- Doped Graphene via Thermal Annealing Graphite Oxide with Melamine and Its Excellent Electrocatalysis, ACS Nano. 5 (2011) 4350–4358.

[51] L. Li, S. Liu, J. Liu, Surface modification of coconut shell based activated carbon for the improvement of hydrophobic VOC removal., J. Hazard. Mater. 192 (2011) 683–90.

[52] T. Sharifi, G. Hu, X. Jia, T. Wagberg, Formation of active sites for oxygen reduction reactions by transformation of nitrogen functionalities in nitrogen-doped carbon nanotubes., ACS Nano. 58 (2013) 1203–1204.

[53] M. Borghei, P. Kanninen, M. Lundahl, T. Susi, J. Sainio, I. Anoshkin, A. Nasibulin, T. Kallio, K. Tammeveski, E. Kauppinen, V. Ruiz, High oxygen reduction activity of few-walled carbon nanotubes with low nitrogen content, Appl. Catal. B Environ. 158–159 (2014) 233–241.

[54] M.S. Dresselhaus, G. Dresselhaus, R. Saito, A. Jorio, Raman spectroscopy of carbon nanotubes, Phys. Rep. 409 (2005) 47.

[55] S. Kundu, W. Xia, W. Busse, M. Becker, D. Schmidth A., M. Havenith, M. Muhler, The formation of nitrogen-containing functional groups on carbon nanotube surfaces: a quantitative XPS and TPD study, Phys. Chem. Chem. Phys. 12 (2010) 4351–4359.

[56] T. Sharifi, F. Nitze, H.R. Barzegar, C.W. Tai, M. Mazurkiewicz, A. Malolepszy, L. Stobinski, T. W??gberg, Nitrogen doped multi walled carbon nanotubes produced by CVD-correlating XPS and Raman spectroscopy for the study of nitrogen inclusion, Carbon N. Y. 50 (2012) 3535–3541.

[57] C. Song, J. Zhang, Electrocatalytic Oxygen Reduction Reaction., PEM Fuel Cell Electrocatal. Catal. Layers Fundam. Appl. (2008) 89–134.

[58] M. Vikkisk, I. Kruusenberg, U. Joost, E. Shulga, I. Kink, K. Tammeveski, Electrocatalytic oxygen reduction on nitrogen-doped graphene in alkaline media, Appl. Catal. B Environ. 147 (2014) 369–376.

[59] T.C. Nagaiah, S. Kundu, M. Bron, M. Muhler, W. Schuhmann, Nitrogen-doped carbon nanotubes as a cathode catalyst for the oxygen reduction reaction in alkaline medium, Electrochem. Comm. 12 (2010) 338–341.

[60] Z. Chen, D. Higgins, Z. Chen, Nitrogen doped carbon nanotubes and their impact on the oxygen

reduction reaction in fuel cells, Carbon N. Y. 48 (2010) 3057–3065.

[61] H.-S. Oh, J.-G. Oh, W.H. Lee, H.-J. Kim, H. Kim, The influence of the structural properties of carbon on the oxygen reduction reaction of nitrogen modified carbon based catalysts, Int. J. Hydrogen Energy. 36 (2011) 8181–8186.

[62] P. Kanninen, M. Borghei, O. Sorsa, E. Pohjalainen, E.I. Kauppinen, V. Ruiz, T. Kallio, Highly efficient cathode catalyst layer based on nitrogen-doped carbon nanotubes for the alkaline direct methanol fuel cell, Appl. Catal. B Environ. 156–157 (2014) 341–349.

[63] Z. Wang, R. Jia, J. Zheng, J. Zhao, L. Li, J. Song, Z. Zhu, Nitrogen-promoted self-assembly of N-doped carbon nanotubes and their intrinsic catalysis for oxygen reduction in fuel cells, ACS Nano. 5 (2011) 1677–1684.

[64] F. Jaouen, M. Lefevre, J.-P. Dodelet, M. Cai, Heat-Treated Fe / N / C Catalysts for O2 Electroreduction : Are Active Sites Hosted in Micropores ?, J. Phys. Chem. B. 110 (2006) 5553–5558..

[65] M. Borghei, Novel carbon nanomaterials for the direct methanol fuel cell electrodes, Aalto University publication series, 2015.

[66] I. Kruusenberg, S. Ratso, M. Vikkisk, P. Kanninen, T. Kallio, A.M. Kannan, K. Tammeveski, Highly active nitrogen-doped nanocarbon electrocatalysts for alkaline direct methanol fuel cell, J. Power Sources. 281 (2015) 94–102.